

Migration velocity analysis by depth image-wave remigration: first results

J. Schleicher, A. Novais, and F.P. Munerato

email: *js@ime.unicamp.br*

keywords: *image-wave, remigration, finite-difference*

ABSTRACT

The image-wave equation for depth remigration is a partial differential equation that is similar to the acoustic wave equation. In this work, we study its finite-difference solution and possible applications. The conditions for stability, dispersion and dissipation exhibit a strong wavenumber dependence. Where higher horizontal than vertical wavenumbers are present in the data to be remigrated, stability may be difficult to achieve. Grid dispersion and dissipation can only be reduced to acceptable levels by the choice of very small grid intervals. Numerical tests demonstrate that, upon reaching the true medium velocity, remigrated images of curved reflectors propagate to the correct depth and those of diffractions collapse to single points. These properties and first applications to inhomogeneous media point towards the method's potential of being useful as a tool for migration velocity analysis. In horizontally layered media, the reflector images reach their true depth when the remigration velocity equals the inverse of the mean medium slowness.

INTRODUCTION

Seismic remigration is an imaging technique that envisages the construction of an improved migrated section for an updated macrovelocity model on the basis of a previously migrated section as obtained with a different initial macrovelocity model. If the two macrovelocity models do not differ too much, one generally calls the imaging procedure that corrects the image a "residual migration" (Rothman et al., 1985). Where significant differences between both models are allowed, the process is referred to as remigration (Hubral et al., 1996) or velocity continuation (Fomel, 1994).

The sequence of images of a certain reflector as subsequently migrated with varying migration velocities creates an impression of a propagating wavefront. This "propagating wavefront" was termed an "image wave" by Hubral et al. (1996). The propagation variable, however, is not time as is the case for conventional physical waves as described, e.g., by the acoustic wave equation, but the migration velocity.

From the kinematic behaviour of these image waves as a function of the constant migration velocity, partial differential equations, termed "image-wave equations," have been derived in 2D (Hubral et al., 1996) and 3D (Mann, 1998). These image-wave equations describe the "propagation" of the reflector image as a function of migration velocity for both, time and depth remigration.

The image-wave equation for *time* remigration has already been theoretically studied and implemented, successfully applied to real data from ground-penetrating radar (Jaya et al., 1999, see also references there). Recently, its use for migration velocity analysis has been discussed by Fomel (2003). The consistency and stability of FD schemes for the 3D image-wave equation for *depth* remigration has been theoretically and numerically studied by Schleicher et al. (2002). Here, we extend that investigation to dispersion and dissipation and discuss the potential of the depth remigration image-wave equation as a technique for migration velocity analysis in homogeneous and vertically inhomogeneous media.

IMAGE-WAVE PROPAGATION

As derived in detail by Mann (1998) and briefly reviewed by Schleicher et al. (2002), the 3D image-wave equation for depth remigration is given by

$$p_{xx} + p_{yy} + p_{zz} + \frac{v}{z}p_{vz} = 0. \quad (1)$$

Here, an index represents a partial derivative with respect to the corresponding variable. Symbol v stands for the actual (constant) value of the migration velocity for a supposedly homogeneous medium. Moreover, $p(x, y, z, v)$ denotes the “image wavefield” as a function of the spatial coordinates and the migration velocity. In other words, $p(x, y, z, v)$ is a depth-migrated section considered as a snapshot of the image-wave propagation.

Variations of this image-wave equation can be obtained by variable transformations of the propagation variable v . Upon replacement of v by $\alpha = v^2$, the differential equation becomes

$$p_{xx} + p_{yy} + p_{zz} + \frac{2\alpha}{z}p_{\alpha z} = 0. \quad (2)$$

Correspondingly, replacement of v by $\beta = \sqrt{v}$ leads to

$$p_{xx} + p_{yy} + p_{zz} + \frac{\beta}{2z}p_{\beta z} = 0. \quad (3)$$

Finally, the most interesting transformation is achieved by replacing v by $\gamma = \ln v$, which yields

$$p_{xx} + p_{yy} + p_{zz} + \frac{1}{z}p_{\gamma z} = 0. \quad (4)$$

In this paper we compare the numerical properties of FD schemes for these equations to those for the original image-wave equation (1).

Finite differences

For the finite-difference schemes, we consider a grid of depth points with initial point at (x_0, y_0, z_0) and a discretized velocity axis with initial value v_0 . The image wavefield at a given grid point $(x_k, y_l, z_m) = (x_0 + k\Delta x, y_0 + l\Delta y, z_0 + m\Delta z)$, as calculated for a certain migration velocity $v_n = v_0 + n\Delta v$, is denoted by $p_{k,l,m}^n$. On this grid, we approximate the derivatives in equation (1) by finite differences. As shown in Schleicher et al. (2002), the reverse forward/forward FD scheme

$$p_{k,l,m}^{n+1} = \frac{z_m \Delta v \Delta z}{v_n} \left\{ \delta_{x,4}^{(2)} p + \delta_{y,4}^{(2)} p + \delta_{z,4}^{(2)} p \right\} + p_{k,l,m+1}^{n+1} - p_{k,l,m+1}^n + p_{k,l,m}^n, \quad (5)$$

and the direct forward/backward FD scheme

$$p_{k,l,m}^{n+1} = -\frac{z_m \Delta v \Delta z}{v_n} \left\{ \delta_{x,4}^{(2)} p + \delta_{y,4}^{(2)} p + \delta_{z,4}^{(2)} p \right\} + p_{k,l,m-1}^{n+1} + p_{k,l,m}^n - p_{k,l,m-1}^n, \quad (6)$$

are stable under certain conditions for increasing and decreasing migration velocity, respectively. Here, the attributes forward/forward and forward/backward refer to the approximation of the mixed derivative in equation (1). Moreover, $\delta_{x,4}^{(2)} p$, $\delta_{y,4}^{(2)} p$, and $\delta_{z,4}^{(2)} p$ denote the fourth-order finite-difference approximations of the spatial second derivatives p_{xx} , p_{yy} , and p_{zz} , respectively, i.e.,

$$\delta_{x,4}^{(2)} p = \frac{1}{12\Delta x^2} \left\{ -p_{k+2,l,m}^n - p_{k-2,l,m}^n + 16(p_{k+1,l,m}^n + p_{k-1,l,m}^n) - 30p_{k,l,m}^n \right\}, \quad (7)$$

with corresponding expressions for $\delta_{y,4}^{(2)} p$, and $\delta_{z,4}^{(2)} p$. The initial condition is given by the original migrated section for the velocity v_0 . As boundary conditions, we use that the field outside the given target zone of the input section should be zero.

Other schemes, particularly those for which the velocity derivative in equation (1) is approximated by a backward difference, did not provide stable results. Equivalent schemes to (6) and (7) were set up for the transformed versions (2) to (4) of the image-wave equation. Below we briefly revisit the corresponding stability conditions and discuss the grid dispersion and dissipation of the stable schemes.

CONSISTENCY, STABILITY, GRID DISPERSION AND DISSIPATION

In order to determine whether an FD scheme can be actually used for a numerical realization of the image-wave propagation, its consistency and stability as well as grid dispersion and dissipation need to be investigated. This may lead to certain conditions for the step size Δv as a function of the medium parameters and the grid intervals Δx , Δy , and Δz . These conditions guarantee that the scheme is stable and suffers less from numerical artifacts. Below, we outline this analysis for schemes (5) and (6).

Consistency and stability

As shown by Schleicher et al. (2002), scheme (5) is unconditionally consistent with the differential equation (1). As can be readily verified by an analogous analysis, the same is true for scheme (6) and the equivalent schemes for equations (2) to (4). To determine the conditions under which these schemes are stable, we apply the von Neumann criterion (see, e.g., Thomas, 1995). It consists of substituting the Fourier component

$$p_{k,l,m}^n = \xi^n \exp\{ik\kappa_x \Delta x\} \exp\{il\kappa_y \Delta y\} \exp\{im\kappa_z \Delta z\} \quad (8)$$

in schemes (5) and (6), where ξ is the so-called amplification factor and κ_x , κ_y , and κ_z are the wavevector components. An FD scheme is known to be stable, if $|\xi| < 1$. The grid dispersion and dissipation are described by the phase and amplitude of ξ , respectively (Strikwerda, 1989).

Substitution of the discrete Fourier transform (8) in equations (5) and (6), and solution of the resulting equation for ξ , yields the expressions

$$\xi = 1 + \frac{2\Lambda}{e^{i\kappa_z \Delta z} - 1} = (1 - \Lambda) - i\Lambda \cot \phi_z \quad (9)$$

and

$$\xi = 1 - \frac{2\Lambda}{e^{-i\kappa_z \Delta z} - 1} = (1 + \Lambda) - i\Lambda \cot \phi_z, \quad (10)$$

respectively, where $\phi_z = \frac{\kappa_z \Delta z}{2}$ and

$$\begin{aligned} \Lambda = & \frac{2z_m}{3v_n} \frac{\Delta v \Delta z}{(\Delta x)^2} \sin^2 \phi_x [3 + \sin^2 \phi_x] + \frac{2z_m}{3v_n} \frac{\Delta v \Delta z}{(\Delta y)^2} \sin^2 \phi_y [3 + \sin^2 \phi_y] \\ & + \frac{2z_m}{3v_n} \frac{\Delta v \Delta z}{(\Delta z)^2} \sin^2 \phi_z [3 + \sin^2 \phi_z]. \end{aligned} \quad (11)$$

The von Neumann condition $|\xi| \leq 1$ provides the stability conditions

$$0 \leq \Lambda \leq 2 \sin^2 \phi_z \quad (12)$$

for scheme (5), and

$$-2 \sin^2 \phi_z \leq \Lambda \leq 0 \quad (13)$$

for scheme (6). Since Λ is directly proportional to Δv , the conditions for the sign of Λ in equations (12) and (13) are immediate conditions for the sign of Δv . We conclude that scheme (5) can only be used for $\Delta v > 0$, i.e., increasing velocities, and scheme (6) only for $\Delta v < 0$, i.e., decreasing velocities. Apart from this difference, the properties of these schemes are sufficiently similar to be discussed at once, using the absolute value $|\Delta v|$.

The presence of the term $\sin^2 \phi_z$ as the limit for Λ in both equations (12) and (13) has an important consequence. It means that FD remigration with schemes (5) and (6) is only possible if the input data are of limited frequency content. If wavenumbers κ_z are present in the data that make $\sin \phi_z$ vanish, no choice for the increments in velocity and space will be possible such that the stability conditions (12) and (13) are met. Even for data with a limited frequency content, care has to be taken to define spatial grids in such a way that for all wavenumbers involved, $\sin \phi_x \approx \sin \phi_y \leq \sin \phi_z$ in order to avoid violations of

conditions (12) and (13). This means that for data where horizontal wavenumbers are larger than vertical ones, a standard square grid will cause instabilities.

We can obtain a rule of thumb for the choice of $|\Delta v|$, if we suppose the grid sizes to be chosen as $\Delta x = \Delta z/\nu_x$ and $\Delta y = \Delta z/\nu_y$ such that $\kappa_x \Delta x \approx \kappa_y \Delta y \approx \kappa_z \Delta z$. In this situation, the above conditions can be divided by $2 \sin^2 \phi_z$ to yield

$$\frac{4}{3} \frac{z_{\max}}{v_{\min}} \nu_x^2 \frac{|\Delta v|}{\Delta z} + \frac{4}{3} \frac{z_{\max}}{v_{\min}} \nu_y^2 \frac{|\Delta v|}{\Delta z} + \frac{4}{3} \frac{z_{\max}}{v_{\min}} \frac{|\Delta v|}{\Delta z} \leq 1 \quad =: \quad |\Delta v| \leq \frac{g}{4} \frac{v_{\min}}{z_{\max}} \Delta z, \quad (14)$$

where we have used that $3 + \sin^2 \frac{\kappa_z \Delta z}{2} \leq 4$. Moreover, we have replaced z_m and v_n by their maximum and minimum values, z_{\max} and v_{\min} , respectively. The grid asymmetry factor g is given by

$$g = \frac{3}{1 + \nu_x^2 + \nu_y^2}. \quad (15)$$

For $\kappa_x \approx \kappa_y \approx \kappa_z$, a square grid can be chosen, and thus $g = 1$. If the layering is predominantly horizontal, the data will contain only small horizontal wavenumbers, i.e., $\kappa_x \approx \kappa_y \ll \kappa_z$. In such a situation, larger horizontal grid sizes can be chosen, which implies small factors ν_x and ν_y and thus a g close to 3.

Grid dispersion and dissipation

For grid dispersion and dissipation, we have to analyze the phase and amplitude of the von Neumann amplification factor ξ , respectively. Expanding both into Taylor series up to second order in $|\Delta v|$ and the spatial grid sizes Δx , Δy , and Δz , we find

$$\arg \xi \approx \pm \left(\frac{\kappa^2 z_m}{\kappa_z v_n} |\Delta v| + \frac{\kappa^4 z_m^2}{2 \kappa_z^2 v_n^2} |\Delta v|^2 \Delta z - \frac{\kappa_z \kappa^2 z_m}{12 v_n} \Delta z^2 |\Delta v| \right), \quad (16)$$

where the upper sign holds for scheme (5) and the lower one for scheme (6), and

$$\ln |\xi| \approx \frac{\kappa^4 z_m^2}{2 \kappa_z^2 v_n^2} |\Delta v|^2 - \frac{\kappa^2 z_m}{2 v_n} \Delta z |\Delta v|. \quad (17)$$

Here, we have introduced κ as defined by $\kappa^2 = \kappa_x^2 + \kappa_y^2 + \kappa_z^2$.

The phase of the amplification factor ξ relates to the (dispersive) image-wave propagation velocity c as

$$c = \frac{\arg \xi}{\kappa \Delta v} \approx \frac{\kappa z_m}{\kappa_z v_n} + \frac{\kappa^3 z_m^2}{2 \kappa_z^2 v_n^2} |\Delta v| \Delta z - \frac{\kappa_z \kappa z_m}{12 v_n} \Delta z^2, \quad (18)$$

and the amplitude of ξ relates to the (exponential) damping coefficient b as

$$b = -\frac{\ln |\xi|}{|\Delta v|} \approx -\frac{\kappa^4 z_m^2}{2 \kappa_z^2 v_n^2} |\Delta v| + \frac{\kappa^2 z_m}{2 v_n} \Delta z. \quad (19)$$

We observe from equation (18) that the image-wave equation possesses intrinsic dispersion since the main term of c depends on the spatial frequencies as κ/κ_z . From equation (19), it becomes clear that the image-wave equation (1) does not possess intrinsic dissipation. In other words, a perfect solution would automatically preserve amplitudes. Moreover, we observe from equations (18) and (19) that b and c depend not only on the wavenumbers κ and κ_z but also on z_m and v_n , i.e., the propagation velocity and the amplitude loss are different at different depths and different migration velocities.

Grid dispersion can be reduced to a minimum even for relatively large values of Δz and Δv , if we can choose these increments in such a way that the second and third terms in expression (18) cancel each other. This implies

$$|\Delta v| = \frac{1}{6} \frac{\kappa_z^2}{\kappa^2} \frac{v_n}{z_m} \Delta z \approx \begin{cases} \frac{1}{6} \frac{v_n}{z_m} \Delta z & \text{if } \kappa_x \approx \kappa_y \approx \kappa_z \\ \frac{1}{18} \frac{z_m}{z_m} \Delta z & \text{if } \kappa_x \approx \kappa_y \ll \kappa_z \\ \frac{1}{6} \frac{v_n}{z_m} \Delta z & \text{if } \kappa_x \approx \kappa_y \ll \kappa_z \end{cases}. \quad (20)$$

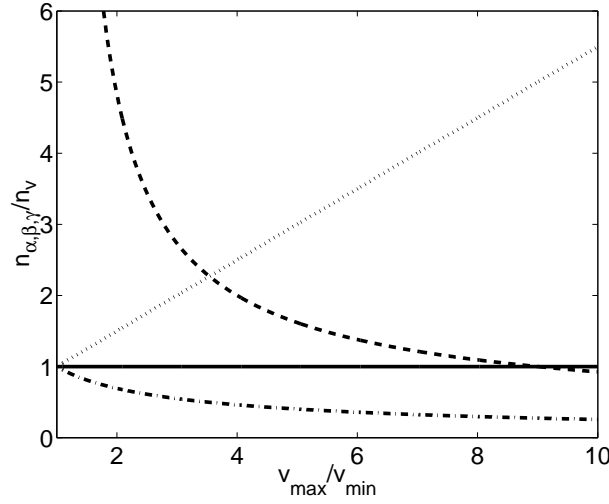


Figure 1: Relative number of necessary steps in variables $\alpha = v^2$ (dotted line) $\beta = \sqrt{v}$ (dashed line) and $\gamma = \ln v$ (dash-dotted line) as a function of v_{max}/v_{min} . The solid line represents the number of steps in v .

In the same way, grid dissipation can be reduced if the increments can be chosen so that the first two term of the Taylor series (19) cancel. This leads to

$$|\Delta v| = \frac{\kappa_z^2 v_n}{\kappa^2 z_m} \Delta z \approx \begin{cases} \frac{1}{3} \frac{v_n}{z_m} \Delta z & \text{if } \kappa_x \approx \kappa_y \approx \kappa_z \\ \frac{v_n}{z_m} \Delta z & \text{if } \kappa_x \approx \kappa_y \ll \kappa_z \end{cases} \quad (21)$$

In fact, we know from the stability analysis above that the latter condition must be corrected by a factor of 3/4 that accounts for the higher terms of the Taylor series. This is because stability means nothing more than that the damping factor b as defined in equation (19) must not become negative. This is guaranteed by conditions (12) and (13).

From the above expressions (20) and (21), we recognize that the best choices for Δv to reduce grid dispersion and dissipation are different. This means that both numerical effects cannot be reduced at the same time by a clever choice of Δv and Δz . Moreover, both dispersion and dissipation depend on the depth and on the migration velocity. In other words, it is impossible to choose Δv and Δz in such a way that dispersion or dissipation would be reduced at all velocity steps and all depths. The only way to achieve an overall improvement of both grid dispersion and dissipation is to choose as small values for Δv and Δz as the increasing computation time allows.

Transformed equations

The corresponding conditions for the forward/forward and forward/backward schemes for the transformed versions (2) to (4) of the image-wave equation can be derived in a completely analogous way. The analysis shows that they can be obtained from the above conditions by a simple substitution of v_n by $2\alpha_n$, $\beta_n/2$, or 1, respectively. As a consequence, their behaviour with respect to stability, grid dispersion, and dissipation does not fundamentally differ from the schemes studied above. All conclusions drawn above for schemes (5) and (6) apply equivalently to the corresponding schemes for the other versions of the image-wave equation.

There is one single difference between these FD schemes for the different versions of equation (1) that is worthwhile mentioning. It concerns the number of steps (and thus computing time) that is necessary to realize a desired remigration between minimum and maximum velocities v_{min} and v_{max} . Upon choosing a step size that exactly satisfies the corresponding stability condition, the numbers of necessary steps for the implementation of each scheme can be compared. In Figure 1, the relative step number for each

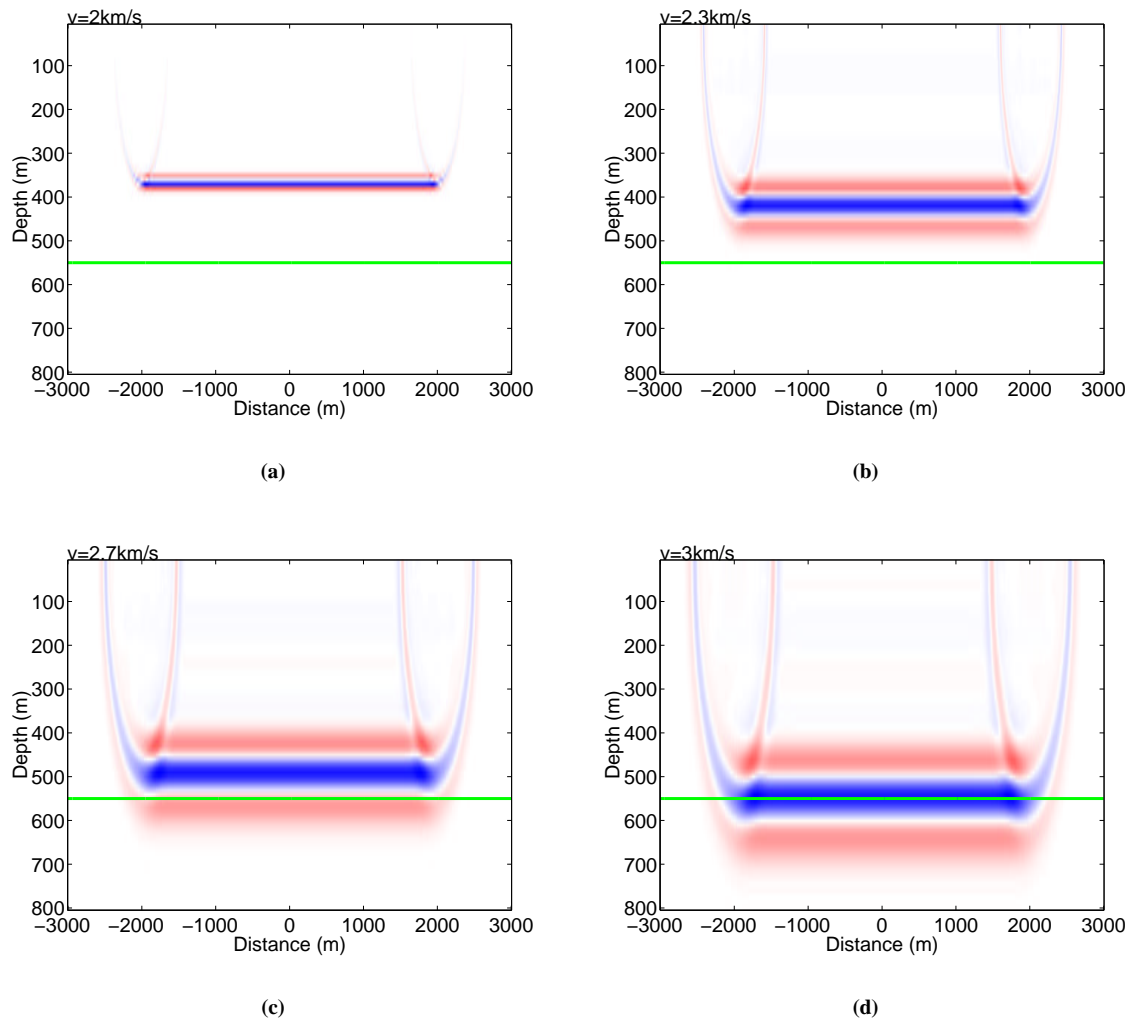


Figure 2: Image wave propagation. Reverse implementation. (a) Input data for the remigration example: data after migration with a wrong migration velocity of $v_0 = 2$ km/s. (b) Remigrated image for $v = 2.3$ km/s. (c) Remigrated image for $v = 2.7$ km/s. (d) Remigrated image for $v = 3.0$ km/s.

variable (normalized with respect to the number of necessary steps in v) is plotted as a function of the ratio v_{max}/v_{min} . We see that of the considered variables, $\gamma = \ln v$ always allows for the fewest steps.

NUMERICAL ANALYSIS

Model 1

To demonstrate the FD image-wave remigration, we had to restrict scheme (5) to the corresponding 2-D one, in order to meet the computational limitations. For the first simple test, we have used ray-synthetic data from a simple earth model consisting of two homogeneous halfspaces, separated by a horizontal reflector at a depth of 550 m. The velocities above and below the reflector are $c_1 = 3$ km/s and $c_2 = 3.5$ km/s. The simulated seismic survey is a zero-offset experiment with 401 source-receiver pairs, located at every 10 m between -2000 m and 2000 m along the x -axis.

The input data to the remigration were generated by a zero-offset depth migration with a wrong migration velocity of $v_0 = 2$ km/s. The resulting depth image is depicted in Figure 2(a). Note that the wrong migration velocity causes the reflector to be imaged at a wrong depth of about 370 m.

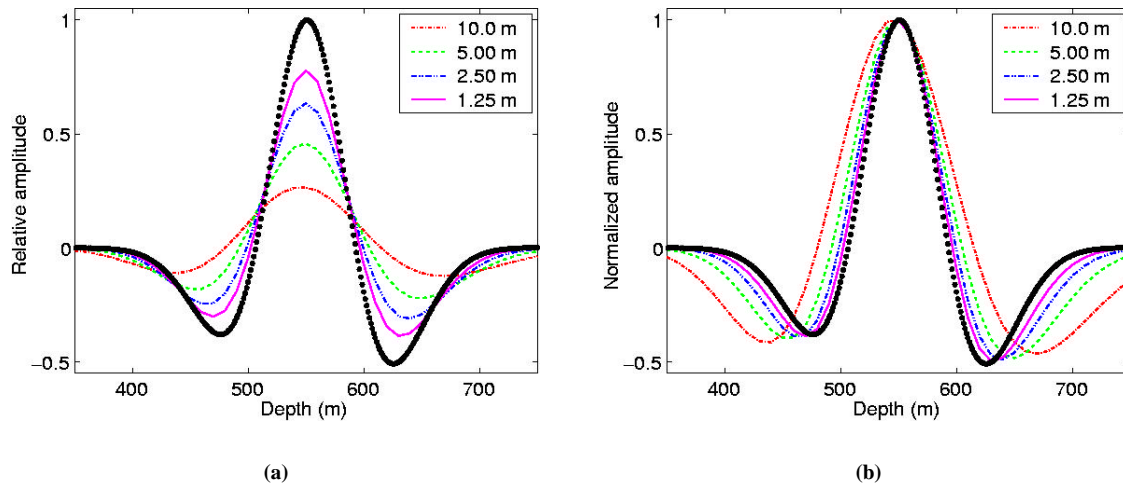


Figure 3: (a) Wavelet at the remigrated reflector image, as obtained with different grid sizes. Observe the amplitude loss due to grid dissipation as a function of grid size as indicated in the upper right corner. The black dotted line represents the reference pulse as obtained from a direct depth migration with the true medium velocity, i.e., without remigration. (b) Same pulses as in (a), scaled to unit amplitude. The pulse stretch, caused by grid dispersion, reduces with decreasing grid size.

This input section was then remigrated using FD scheme (5). The grid size of the depth region was $\Delta x = \Delta z = 10$ m and the velocity increment was $\Delta v = 4$ m/s. This is in accordance with the 2-D version of stability condition (14) (where the factor $1/4$ is replaced by $3/8$). Parts (b), (c), and (d) of Figure 2 show the snapshots of the image wave for velocities $v = 2.3$ km/s, $v = 2.7$ km/s, and $v = 3.0$ km/s, respectively, the latter being the true medium velocity. We observe that the reflector image in Figure 2(d) is remigrated to the correct depth of 550 m.

As a final observation, let us comment on the pulse stretch of FD remigration (Figure 2). It is much stronger than the conventional pulse stretch due to depth migration, which is proportional to the migration velocity (Tygel et al., 1994). The reason for the additional stretch is the grid dispersion as theoretically discussed above.

Figure 3 numerically demonstrates the effects of grid dispersion and dissipation. It shows the pulse across the remigrated horizontal reflector image at the true medium velocity and depth, as obtained by remigration with different grid sizes. All images were obtained from the same synthetic zero-offset data by a depth migration with the wrong velocity $v_0 = 2$ km/s onto a depth grid of different step sizes and a subsequent remigration to the correct velocity of 3 km/s. The grossly dotted reference curve is the pulse as obtained from a direct true-amplitude depth migration with the true medium velocity.

In Part (a) of Figure 3, all pulses are depicted with relative amplitudes scaled with respect to the reference pulse. The different amplitudes of the different pulses demonstrate the increasing dissipation for larger grid increments in depth. In all remigrations, Δv was chosen accordingly so as to obey the respective stability condition. Part (b) of Figure 3 depicts the same pulses as Part (a), however scaled to unit amplitude. The stretch effect as a consequence of grid dispersion clearly reduces with decreasing grid size. Note that the remigration with $\Delta x = \Delta z = 1.25$ m took about 500 times longer than the one with $\Delta x = \Delta z = 10$ m.

Model 2

To study the effect of finite-difference image-wave depth remigration on dipping and curved interfaces, we have devised Model 2. It consists of a constant-velocity background model with wavespeed 3.0 km/s and three interfaces of different shape representing density contrast. The curved top reflector separates the upper half-space with density 1 g/cm^3 from the first layer with density 2 g/cm^3 . The second layer with

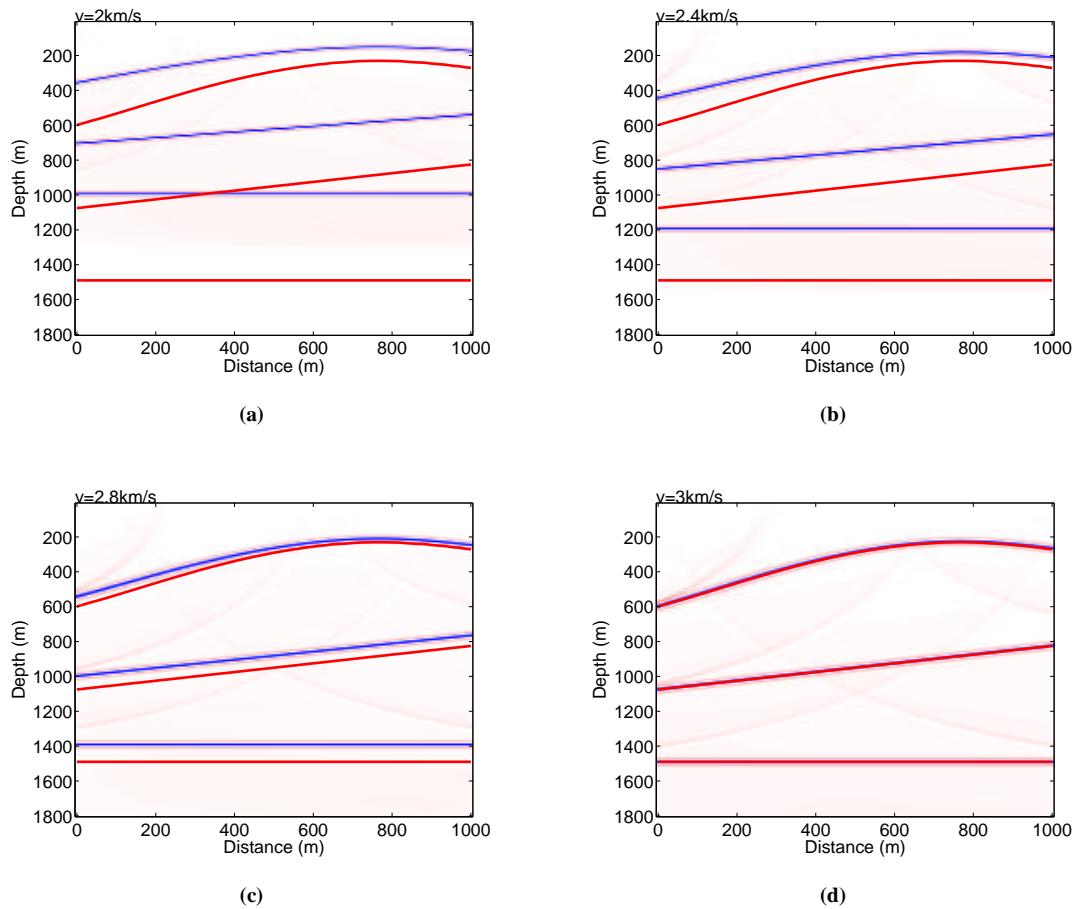


Figure 4: Image wave propagation with the forward/forward FD scheme from $v_{\text{mig}} = 2.0$ km/s to $v_{\text{mig}} = 3.0$ km/s.

density 4 g/cm^3 is separated from the first one by a planar interface that dips to the left, and from the lower half-space with density 8 g/cm^3 by a horizontal reference reflector at a depth of 1500 m. The densities were chosen so as to guarantee equal reflection coefficient at all interfaces.

In this model, a synthetic zero-offset section was simulated by 2.5D ray modelling using the Norsar ray tracer without transmission loss. Coincident source-receiver pairs were regular distributed along the x -axis between -500 m and 1500 m. These synthetic data were depth-migrated onto a $10 \text{ m} \times 10 \text{ m}$ depth grid by constant-velocity true-amplitude Kirchhoff migration, using the (wrong) migration velocity 2 km/s. The resulting migrated image is depicted in Figure 4(a). Superimposed are the correct positions of the reflectors. These migrated data have then been subjected to an FD remigration with the forward/forward scheme (5) that allows for increasing remigration velocities. To guarantee stability and reduce grid dispersion we have chosen a step size of $\Delta v = 0.2 \text{ m/s}$. Figures 4(b) to (d) show snapshots of the resulting image-wave propagation at remigration velocities 2.4 km/s, 2.8 km/s and 3.0 km/s. Observe the perfect coincidence between the remigrated reflector images and the true reflector positions at the correct velocity of 3.0 km/s.

A corresponding test was carried out with the forward/backward FD scheme. For this purpose, the same synthetic data were migrated with a too high migration velocity of 4.0 km/s. FD remigration was then applied toward lower velocities. Figure 5 shows four snapshots of the corresponding image-wave propagation. Again, when the remigration velocity reaches the true medium velocity of 3.0 km/s, the coincidence of the reflector images and their correct positions in depth is perfect.

Note that for remigration in the direction of decreasing velocities, a larger step size of $\Delta v = -2 \text{ m/s}$

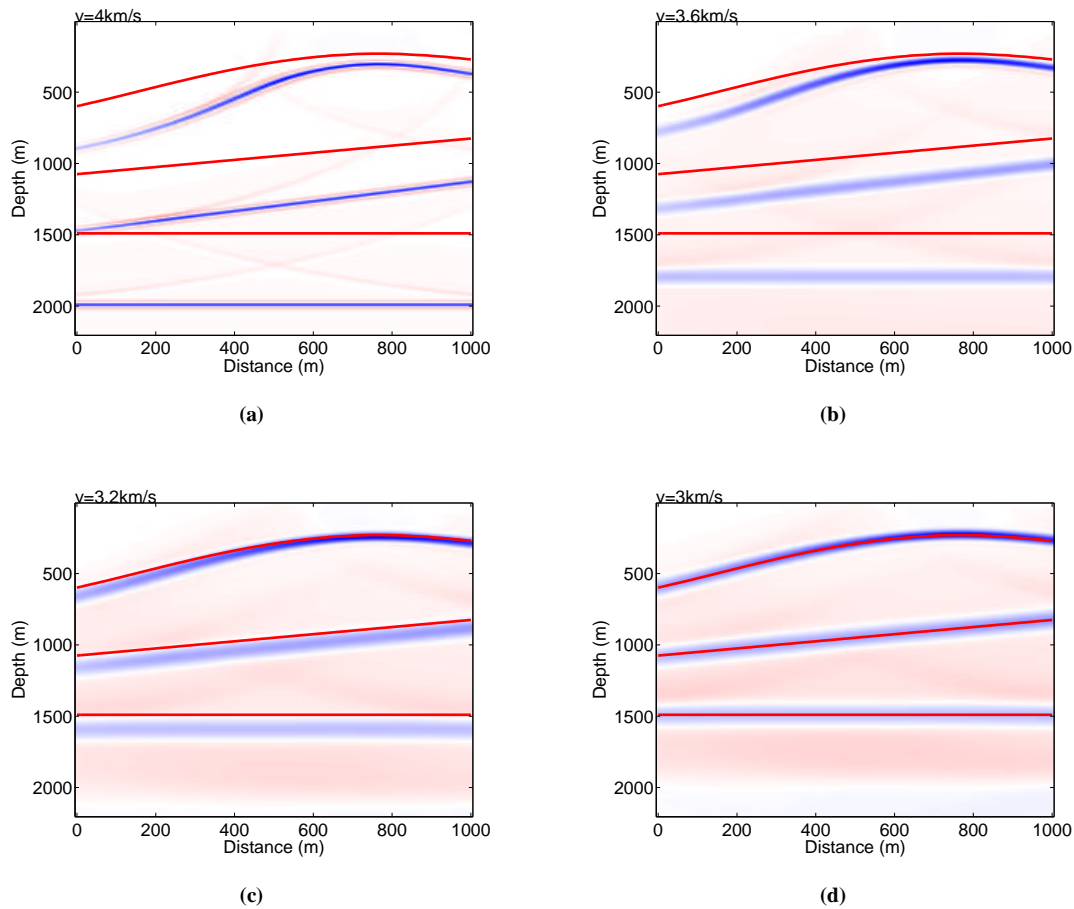


Figure 5: Image wave propagation with the forward/backward FD scheme from $v_{\text{mig}} = 4.0$ km/s to $v_{\text{mig}} = 3.0$ km/s.

could be chosen. The reason is that the intrinsic dispersion of the image-wave equation, which describes the correct migration pulse stretch, now causes a contraction of the pulse. In this way it has the opposite effect to grid dispersion, which tends to enlarge the pulse. Therefore, the overall pulse stretch is considerably reduced for propagation to lower velocities. In fact, attention has to be paid not to choose Δv too small, so as to avoid problems with the wavenumber content of the pulse becoming too high for equation (12) to be satisfied. Such problems have been reported by Mann (1998).

Model 3

After having confirmed that FD image-wave remigration indeed propagates curved reflectors to their correct position in depth when the true remigration velocity is reached, our next objective is to use this property for velocity analysis. If the true reflector depth at some point (e.g., at a borehole) is a priori known, FD image-wave remigration can be used to detect the best migration velocity. Unfortunately, this is not generally the case. Therefore, we need another way of detecting the previously unknown best migration velocity by remigration, a way that must not rely on the knowledge of the reflector depth. A possibility is demonstrated by Model 3, which consists of a single diffraction point at a depth of 550 m in a constant-velocity background with $v = 3.0$ km/s (see Figure 6).

For this model, synthetic ray data have been simulated and then depth-migrated with the same parameters as before. The sequence of remigration snapshots in Figure 7 shows that the wrongly migrated diffraction nicely collapses at the true medium velocity into a single point at the correct depth and then de-

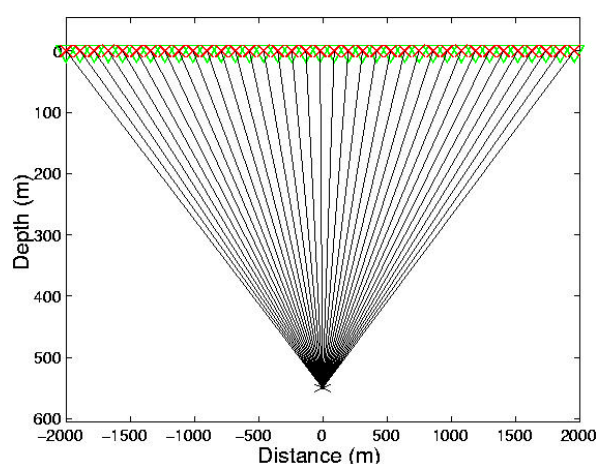


Figure 6: Model with a single diffraction point at depth 550 m in a homogeneous background model with $v = 3.0$ km/s.

focuses again. It is easy to determine from this sequence of snapshots that the true medium velocity for this model must be close to 3 km/s. In conclusion, it is possible to use such a sequence of images to determine the best migration velocity from FD image-wave remigration if visible diffraction events are present in the migrated zero-offset data.

Model 4

Up to now, we have applied the FD image-wave depth remigration only in constant-velocity models, for which its theory has been developed. To be of actual practical use, however, the technique needs to be extended to inhomogeneous media. With Model 4, we investigate whether the same image-wave remigration equation can be applied in horizontally layered media and what would be the meaning of the remigration velocity in such a situation.

The model consists of two homogeneous layers between two homogeneous halfspaces, separated by horizontal reflectors at depths of 200 m, 650 m, and 1550 m. The velocities in the halfspaces and layers are, from top to bottom, $v_1 = 2.0$ km/s, $v_2 = 3.0$ km/s, $v_3 = 6.0$ km/s, and $v_4 = 12.0$ km/s. The simulated seismic survey is again a zero-offset experiment with 401 source-receiver pairs, located at every 10 m between -2000 m and 2000 m along the x -axis. The synthetic data have been modelled by the 2.5D finite-difference solver of the acoustic wave equation of Novais and Santos (2002).

The input data to the remigration were generated by a zero-offset depth migration with a wrong migration velocity of $v_0 = 1.5$ km/s. The resulting depth image is depicted in Figure 8a. Also indicated are the true depths of the three horizontal reflectors. Note that the too low migration velocity causes the reflectors to be imaged at too shallow depths.

This input section was then remigrated using FD scheme (5). The grid size of the depth region was $\Delta x = \Delta z = 5$ m and $\Delta v = 0.2$ m/s. The actual value of Δv was chosen smaller than indicated by stability condition (14), in order to reduce the effects of grid dispersion and dissipation in accordance with formulas (20) and (21). The parts of Figure 8 shows the original migrated image at $v = 1.5$ km/s and three snapshots of the image wave for velocities $v = 2.02$ km/s, $v = 2.62$ km/s, and $v = 3.90$ km/s. The depicted images are those where the migrated images of the reflectors seem to be correctly positioned in depth. We refer to the corresponding velocity values as “focusing velocities”. To confirm that at these velocities, the reflector images are at the right depth, we look at a single depth trace. Figure 9(a) shows three remigrated pulses from the center of the image at the velocities of 2.00 km/s, 2.02 km/s, and 2.04 km/s. The pulse for 2.02 km/s seems to be best positioned at the true depth of the first reflector indicated by a vertical line. Correspondingly, Figures 9(b) and 9(c) show three remigrated pulses at velocities of 2.60 km/s, 2.62 km/s, and 2.64 km/s as well as 3.88 km/s, 3.90 km/s, and 3.92 km/s, respectively. In each of these Figures, a solid black line indicates the true depth of the corresponding reflector.

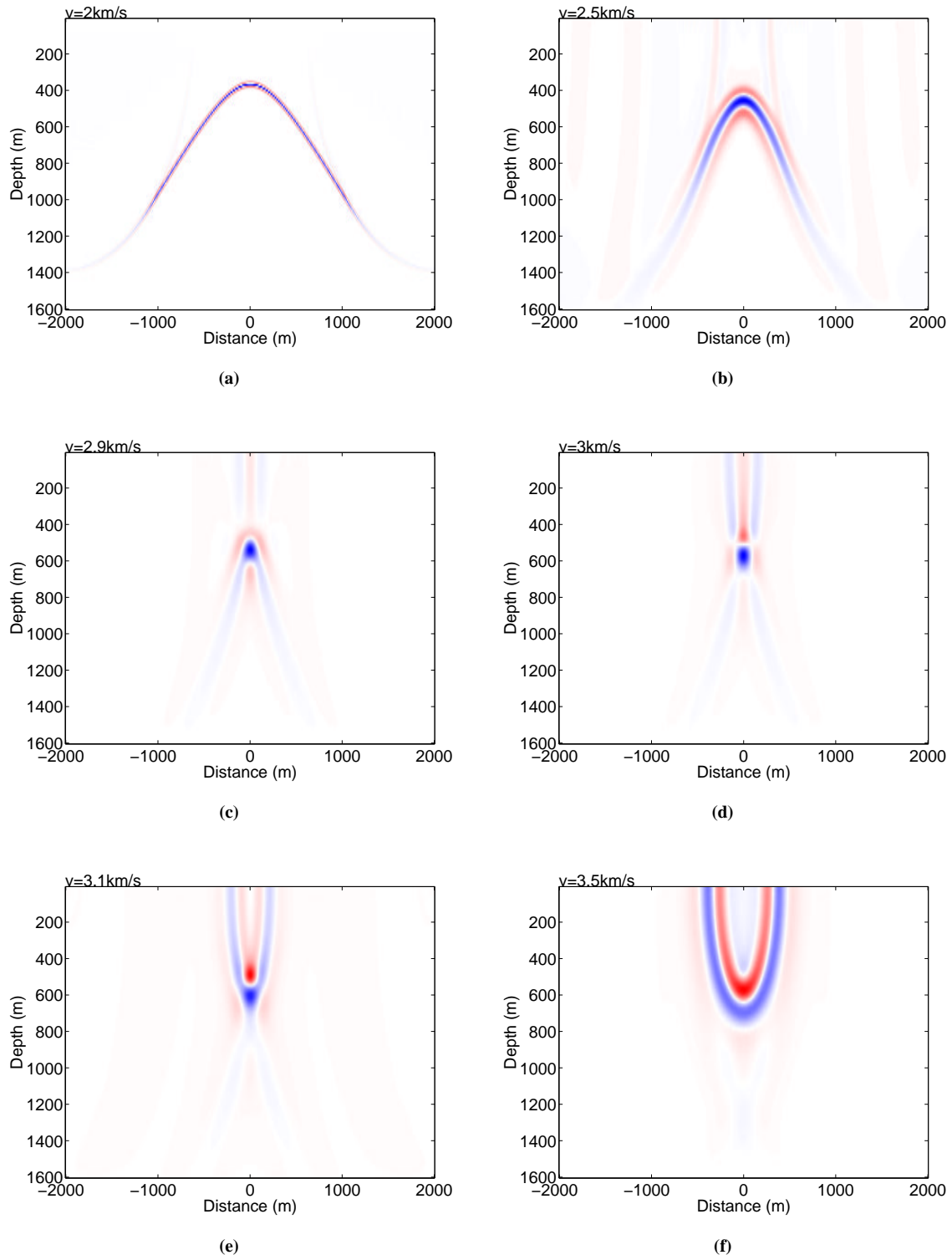


Figure 7: Image wave propagation of the image of a diffraction point. (a) Input data for the remigration example: diffraction data after migration with a wrong migration velocity of $v_0 = 2$ km/s. (b) Remigrated image for $v = 2.5$ km/s. (c) Remigrated image for $v = 2.9$ km/s. (d) Remigrated image for $v = 3.0$ km/s. The image of the diffraction collapses into a point. (e) Remigrated image for $v = 3.1$ km/s. (f) Remigrated image for $v = 3.5$ km/s.

Reflector No.	focusing velocity	mean slowness velocity	rms velocity	mean velocity
1	2.02	2.0000	2.0000	2.0000
2	2.62	2.6000	2.6458	2.6923
2	3.90	3.8750	4.2279	4.6129

Table 1: Comparison of average velocities and focusing velocities.

To understand the focusing velocities, we have calculated three different types of average velocities for the three reflectors, these being the mean velocity, the inverse of the mean slowness and the rms velocity. The theoretical values of these average velocities at the reflector depths are summarized in Table 1. Note the almost perfect coincidence between the theoretical values of the mean slowness velocities and the migration velocities that remigrate the reflectors to the correct depths. The reason for the fact that the focusing velocities are slightly higher than the mean slowness velocities is probably the slight asymmetry of the migrated pulse. This coincidence confirms the claim that image-wave remigration has the potential to be used in vertically inhomogeneous media for migration velocity analysis. Depending on the average slowness rather than rms velocity, it can provide an independent measure of interval velocities. Further investigations will have to show how far the concept can be stretched to laterally inhomogeneous media.

As a final observation on grid dispersion and dissipation, let us stress the fact that these effects are much stronger in Figure 8 for the deeper reflectors than for the shallower ones. This is in accordance with equations (16) and (17) which predict both effects to be increasing with depth.

CONCLUSIONS

The image-wave equation for depth remigration is a second-order partial differential equation that describes the “propagation” of a migrated reflector image as a function of a changing migration velocity (Fomel, 1994; Hubral et al., 1996). In this work, we have revisited the stability conditions of two FD schemes for this equation. The theoretical stability condition obtained from the von Neumann criterion points toward general difficulties of the process when remigrating data containing unlimited frequency content. For large wavenumbers in the horizontal directions, care has to be taken to define the grid sizes accordingly.

With the investigated FD schemes, reflector images can be remigrated only either to larger or to smaller migration velocities. The scheme forward in v and forward in z allows only for an increase, the scheme forward in v and backward in z only for a decrease of the migration velocity. Other FD schemes with different approximations of the mixed derivative have not produced stable results.

The theoretical studies of the stable FD schemes have been extended to grid dispersion and dissipation. We have seen that image-wave propagation suffers from intrinsic dispersion as well as grid dispersion and dissipation due to chosen FD scheme. The theoretical analysis has shown that the latter effects depend on velocity and depth as well as on the spatial frequencies. Therefore, they cannot be entirely eliminated for all frequencies, depths, or velocities by an appropriate choice of the grid size. They can only be reduced by choosing the grid size as small as possible.

Transformations of the depth-remigration image-wave equation with respect to the propagation variable, i.e., migration velocity, have not brought any improvements with respect to stability, dispersion, or dissipation. The only advantage of such a transformation was found to be a speedup of the corresponding implementation because of a reduction of the necessary number of steps.

Several numerical examples have been presented that exhibit the properties of FD image-wave remigration. Using a homogeneous model with a single reflector, the dependency of the grid dispersion and dissipation on the grid size has been demonstrated. With the help of a three-reflector constant-velocity model, image-wave propagation to higher and lower velocities has been shown to work well also for dipping and curved reflectors.

By application of the remigration image-wave equation to synthetic data of a single diffraction event, we have seen that such an event collapses to a single point at the true medium velocity, thus enabling the detection of this velocity independently of other means. This is an encouraging result as it indicates how remigration might be employed as a tool for migration velocity analysis.

Moreover, we have demonstrated that the method, although strictly valid for homogeneous media only,

can be applied in vertically inhomogeneous media. A propagating reflector image reaches its true depths at a migration velocity that approximately equals the inverse of the mean slowness. In this way, mean slownesses can be determined from image-wave remigration, thus enabling a new way of migration velocity analysis. Further investigations will have to show how far the concept can be stretched to laterally inhomogeneous media.

ACKNOWLEDGEMENTS

This work was kindly supported by the CNPq and FAPESP, Brazil, and the sponsors of the *Wave Inversion Technology (WIT) Consortium*, Karlsruhe, Germany.

REFERENCES

- Fomel, S. (1994). Method of velocity continuation in the problem of seismic time migration. *Russian Geology and Geophysics*, 35(5):100–111.
- Fomel, S. (2003). Time migration velocity analysis by velocity continuation. *Geophysics*, 68(5):1662–1672.
- Hubral, P., Tygel, M., and Schleicher, J. (1996). Seismic image waves. *Geophys. J. Internat.*, 125(2):431–442.
- Jaya, M., Botelho, M., Hubral, P., and Liebhardt, G. (1999). Remigration of ground-penetrating radar data. *J. Appl. Geoph.*, 41:19–30.
- Mann, J. (1998). Derivation and implementation of the seismic image wave theory and its application to seismic reflection data. Master's thesis, Universität Karlsruhe (TH).
- Novais, A. and Santos, L. (2002). 2.5-D finite difference solution of the acoustic wave equation. *WIT Report*, 6:252–261.
- Rothman, D., Levin, S., and Rocca, F. (1985). Residual migration: Applications and limitations. *Geophysics*, 50(1):110–126.
- Schleicher, J., Novais, A., and Munerato, F. (2002). Finite-difference solution of the image wave equation for depth remigration: stability. *WIT Report*, 6:107–117.
- Strikwerda, J. (1989). *Finite Difference Schemes and Partial Differential Equations*. Wadsworth & Brooks, California.
- Thomas, J. (1995). *Numerical Partial Differential Equations*. Springer-Verlag, New York.
- Tygel, M., Schleicher, J., and Hubral, P. (1994). Pulse distortion in depth migration. *Geophysics*, 59(10):1561–1569.

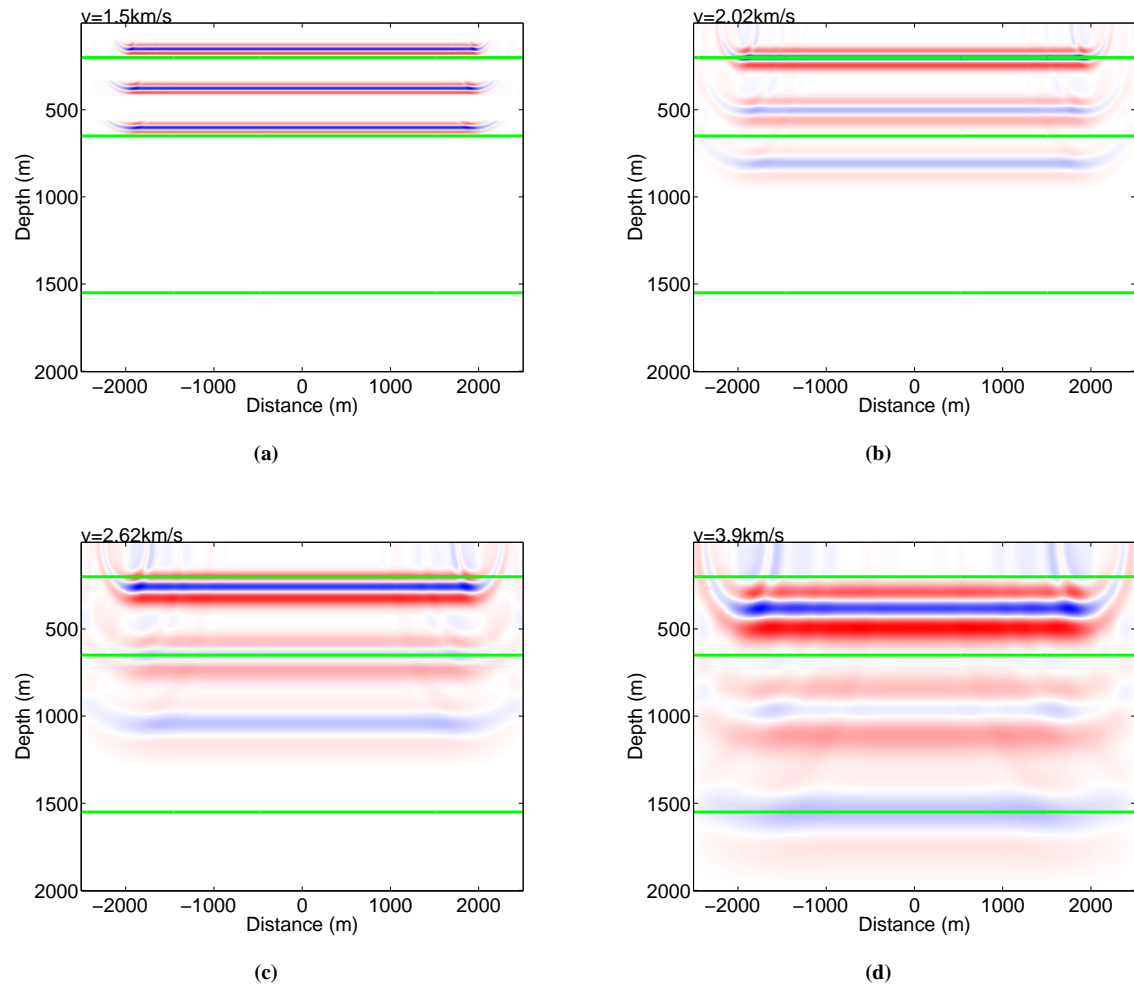


Figure 8: Image wave propagation in a vertically inhomogeneous medium. (a) Input data for the remigration example: data after migration with a wrong migration velocity of $v_0 = 1.50$ km/s. (b) Remigrated image for $v = 2.02$ km/s. The first reflector is imaged at the correct depth. (c) Remigrated image for $v = 2.62$ km/s. The second reflector is imaged at the correct depth. (d) Remigrated image for $v = 3.90$ km/s. The third reflector is imaged at the correct depth.

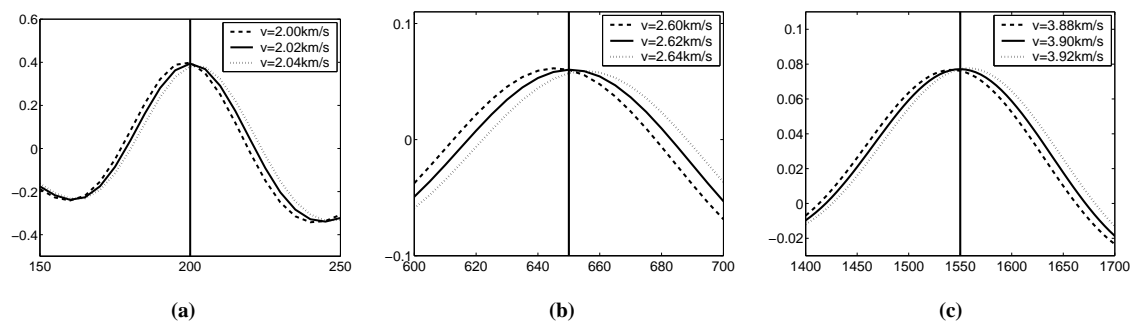


Figure 9: Migrated pulses at different velocities. Best migration velocities are those where the center of the pulse is at the true reflector depth. (a) First reflector. (b) Second reflector. (c) Third reflector.